2022「中技社科技獎學金」

2022 CTCI Foundation Science and Technology Scholarship

境外生研究獎學金

Research Scholarship for International Graduate Students

Study on Electrochemical Sensors for Real-time In-situ Monitoring of Intracellular Signaling Molecules in Cancer Cells

Asit Kumar Panda, 4th Year Ph.D. Student, Advisor-Ren-Jei Chung

Department of Chemical Engineering & Biotechnology, National Taipei University of Technology, Taipei, Taiwan

Abstract

Here, high catalytic NP/composites such as PtNi NPs, N-GQDs@SnS_2, and PtNi@N-GQDs were prepared for application in electrochemical sensors for H_2S, H_2O_2, and Dopamine(DA), scrutinized using various techniques including XRD, Raman, UV-Vis, XPS, TEM, FESEM, EDX, and elemental mapping analysis to understand the structural moiety, morphology, a and elemental composition of synthesized nanomaterials. In this aspect,(1)a disposable electrochemical sensor based on PtNi NPs(5.6 nm) for sensitive and specific in situ monitoring of H_2S released by human breast cancer cells. The PtNi alloy NPs modified electrode was applied for in situ monitoring of H_2S secreted by human breast cancer cells. (2) Design and construction of enzyme-free sensors using N-GQDs (less than 1 nm)-decorated SnS2 were proposed for in situ monitoring of H_2O_2 secreted by human breast cancer cells. The resulting hybrid material was an excellent electrocatalyst for reducing H_2O_2 molecules.(3) Moreover enzyme-free sensor was designed using PtNi NPs conjugated N-GQDs for sensitive and highly specific in situ monitoring of DA secreted by rats C6 cells.

Electrochemical sensor based on PtNi NPs for in situ monitoring of H_2S in breast cancer cells

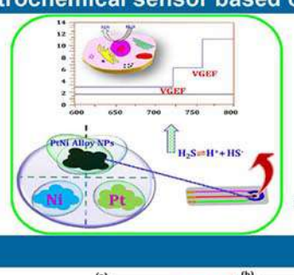

Figure 1. Schematic representation of PtNi alloy NP formation and electrochemical detection of H_2S in a human breast cancer cell

Characterization

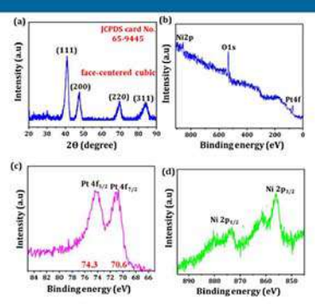

Figure 2. (a) XRD pattern of PtNi NPs, (b) survey spectrum of PtNi NPs, magnified XPS profiles of (c) Pt 4f and (d) Ni 2p

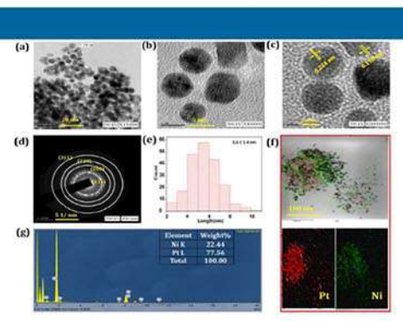

Figure 3. (a) TEM image, (b and c) HRTEM images, (d) selected area electron diffraction (SAED) pattern, (e) particle size distribution, (f) EDX mapping images, (g) EDX spectrum of PtNi NPs (insert: elemental weight percentage).

Electrochemical determination of H_2S at PtNi

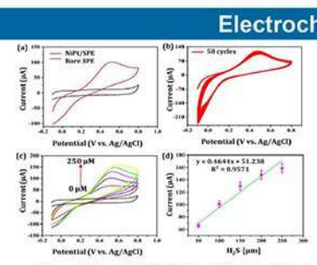

Figure 4. (a) CV curves of bare SPE and PtNi/SPE for 100 µM sulfide in 0.05 M PB (pH 7.0) at a scan rate of 0.05 V s^{-1}, (b) 50 consecutive CV cycles of PtNi/SPE in 0.05 M PB (pH 7.0) containing 100 µM of sulfide at a scan rate of 0.05 V s^{-1}, (c) CV curves of different concentrations of sulfide (0–250 µM) at PtNi/SPE in 0.05 M PB (pH 7.0), (d) calibration plot of I_{pa} vs. concentration (µM) of sulfide.

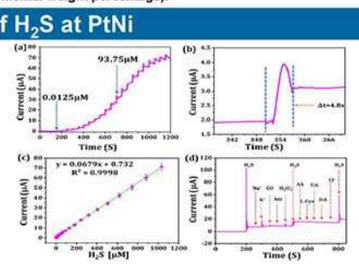

Figure 5. (a) Amperometry (i-t) response of various concentrations of sulfide (0.0125–1031 µM) in 0.05 M PB (pH 7.0), (b) response time for steady-state current, (c) corresponding linear plot for Ipa vs. [sulfide] (d) effect of interfering species Na^+, K^+, CO, NO, hydrogen peroxide (H_2O_2), ascorbic acid (AA), L-cysteine (L-cys), uric acid (UA), dopamine (DA), and Cl^- on the amperometric responses of PtNi/SPE for sulfide in 0.05 M PB (pH 7.0).

Detection of H_2S released in live cells

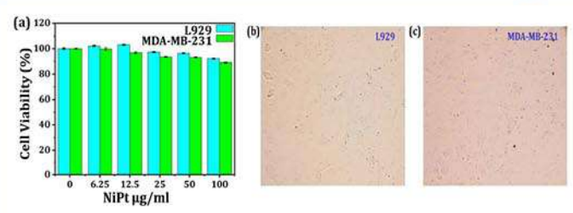

Figure 6. (a) Cell viability of L929 and MDA-MB-231 cells, microscopic images of (b) L929 and (c) MDA-MB-231 cells

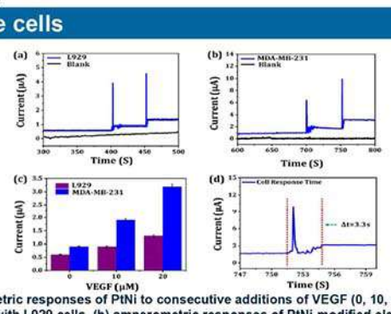

Figure 7. (a) Amperometric responses of PtNi to consecutive additions of VEGF (0, 10, and 20 µM) without L929 and with L929 cells, (b) amperometric responses of PtNi-modified electrode to consecutive additions of VEGF (0, 10, and 20 µM) without MDA-MB-231 and with MDA-MB-231 cells in 0.05 M PB at 0.49 V, (c) corresponding current response between L929 and MDA-MB-231 cells with various concentrations of VEGF, (d) amperometric response time for H_2S released from cancer cells

Electrochemical Sensor Based on N-GQDs@SnS_2 for In Situ Monitoring of H_2O_2 in Breast Cancer Cells

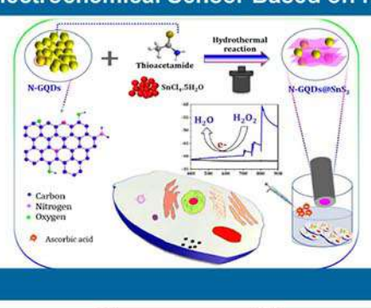

Figure 8. Schematic representation of N-GQDs/SnS_2 composite formation and electrochemical detection of H_2O_2 in human breast cancer cells.

Characterization

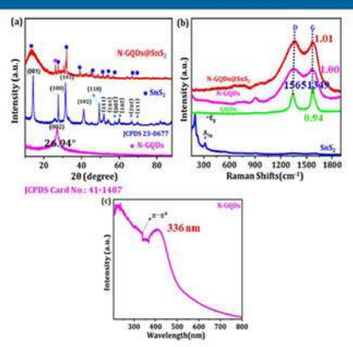

Figure 9. (a) XRD patterns of N-GQDs, SnS_2, and N-GQD@SnS_2 and (b) Raman spectra of GQDs, SnS_2, and N-GQD@SnS_2; (c) UV-vis absorption spectra of N-GQDs.

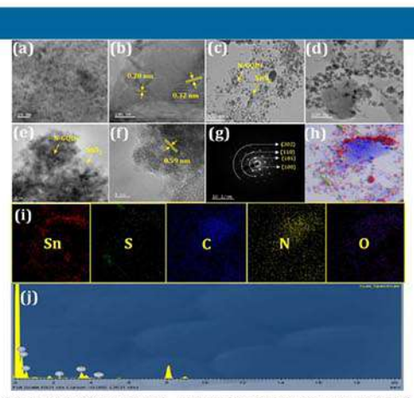

Figure 10. TEM images of (a) N-GQDs, (b) SnS_2, FESEM-based morphology of (c) SnS_2, (d) N-GQDs@SnS_2. TEM images of (e and f) N-GQDs@SnS_2, (g) SAED pattern of N-GQDs@SnS_2, (h) TEM-EDX mapping images of N-GQDs@SnS_2 nanocomposite, and (i) the corresponding EDX spectrum of N-GQDs@SnS_2

Electrochemical determination of H_2O_2 at N-GQDs@SnS_2

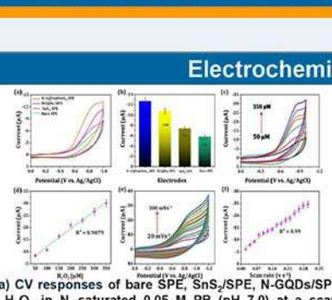

Figure 11. (a) CV responses of bare SPE, SnS_2/SPE, N-GQDs/SPE, and N-GQD@SnS_2/SPE for 100 µM H_2O_2 in N_2-saturated 0.05 M PB (pH 7.0) at a scan rate 0.05 V s^{-1}, (b) the corresponding bar graph for reduction current versus different electrodes (c) CV response of N-GQDs@Sn_{52}/SPE for various concentrations of H_2O_2 (50–350 µM), (d) linear plot of I_{pa} and concentration of H_2O_2 (µM). (e) CV response of N-GQDs@SnS_2/SPE for 100 µM H_2O_2 at various scan rates (0.02–0.3 V s^{-1}), (f) linear plot for the I_{pc} of H_2O_2 and scan rates (Vs^{-1})

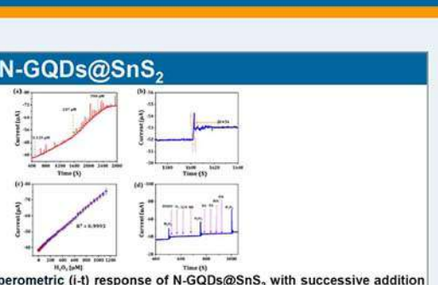

Figure 12. (a) Amperometric (i-t) response of N-GQDs@SnS_2 with successive addition of H_2O_2 (0.0125–1128 µM) at -0.86 V; (b) response time for steady-state current; (c) calibration plot of I_{pc} versus H_2O_2 concentrations; (d) effects of interfering species such as Na^+, K^+, glucose (GLU) sucrose (SUC), L-cysteine (L-cys), ascorbic acid (AA), uric acid (UA), and dopamine (DA) on the amperometric responses of N-GQDs@SnS_2 for H_2O_2 in N_2-saturated 0.05 M PB (pH 7.0).

Detection of H_2S released in live cells

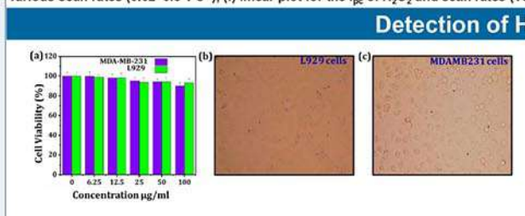

Figure 13. (a) Viability of MDA-MB-231 and L929 cells; microscopic images of (b) MDA-MB-231 and (c) L929 cells.

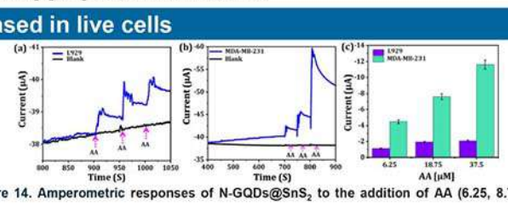

Figure 14. Amperometric responses of N-GQDs@SnS_2 to the addition of AA (6.25, 8.75, 37.5 µM) in 0.05 M PB at −0.86 V (a) without MDA-MB-231 cells and with MDA-MB-231 cells (b) without L929 and with L929 cells. (c) Corresponding current responses for MDA-MB-231 and L929 cells with varying concentrations of AA.

Electrochemical Sensor Based on PtNi@N-GQDs for In Situ Monitoring of Dopamine in Glioma Cells

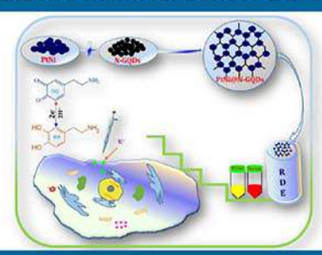

Figure 15. Schematic representation of PtNi@N-GQDs composite formation and electrochemical detection of DA in C6 cells

Characterization

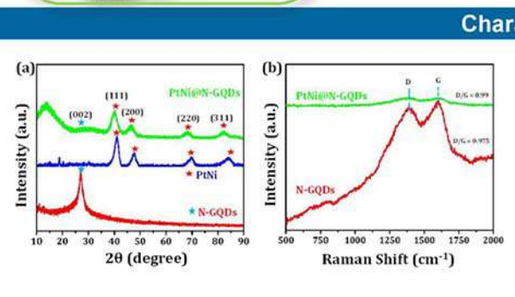

Figure 16. (a) XRD pattern of N-GQDs, PtNi, and PtNi@N-GQDs, (b) Raman spectra of N-GQDs, and PtNi@N-GQDs.

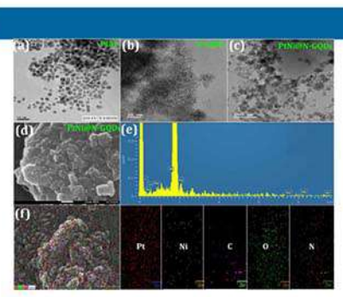

Figure 17. TEM image of (a) PtNi, (b) N-GQDs, and (c) PtNi@N-GQDs. FESEM images of (d) PtNi@N-GQDs, (e) EDX spectrum of PtNi@N-GQDs, and (f) FESEM-EDX mapping images of PtNi@N-GQDs nanocomposite.

Electrochemical determination of DA AT PTNI@N-GQDs

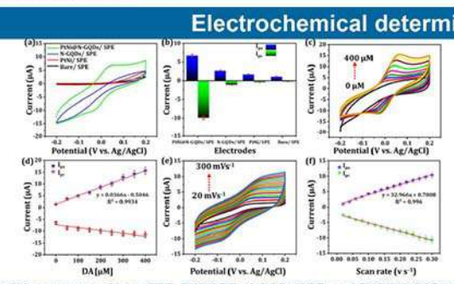

Figure 18. (a) CV responses of bare SPE, PtNi/SPE, N-GQDs/SPE, and PtNi@N-GQDs/SPE for 100 µM DA in 0.05 M PB at 0.05 V s^{-1}, (b) the bar diagram for Ip of DA versus different modified SPEs, (c) CVs of PtNi@N-GQDs/SPE for successive addition of DA (0–400 µM), (d) linear plot of Ip and concentration of DA (µM), (e) CVs of PtNi@N-GQDs/SPE for 100 µM DA at scan rates from 0.02 V s^{-1} to 0.3 V s-1), (f) linear plot for the Ip of DA and scan rates (Vs^{-1}).

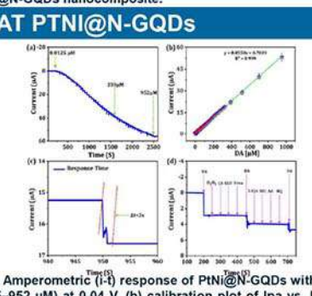

Figure 19. (a) Amperometric (i-t) response of PtNi@N-GQDs with consecutive addition of DA (0.0125–952 µM) at 0.04 V, (b) calibration plot of Ipa vs. DA concentrations, (c) response time for steady-state current, (d) effects of interfering species such as H_2O_2, caffeic acid (CA), glucose (GLU), urea, L-cysteine (L-cys), sucrose (SUC), ascorbic acid (AA), and hydroquinone (HQ) on the responses of PtNi@N-GQDs for DA in PB.

Detection of DA released by glioma cells

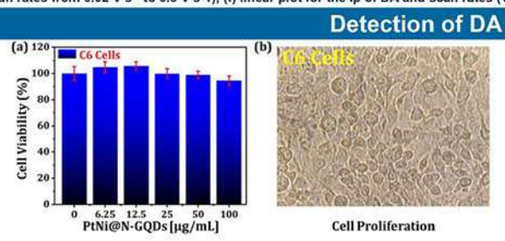

Figure 20. (a) Viability of C6 cells and microscopic images of (b) C6 cells.

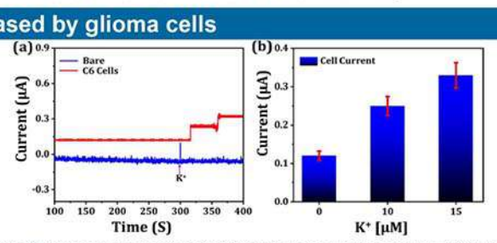

Figure 21. Amperometric result of PtNi@N-GQDs to the addition of K^+ ions (0, 10, 15 µM) in PB at 0.04 V (a) without C6 cells and with C6 cells, (b) Corresponding current responses for C6 cells with varying concentrations of K^+ ions.

Conclusion

Herein, reported simple and unique approaches to fabricate different electrodes PtNi, N-GQDs@SnS_2, and PtNi@N-GQDs using a simple hydrothermal method. The TEM, FESEM, EDX, XRD, Raman, UV-vis, and XPS observations confirmed the effective formation of the nanoparticles and nanocomposite. The nanomaterials modified with SPE were exploited as a potential enzyme-free electrochemical sensor for the determination of the signaling molecules. Moreover, these sensors displayed superior analytical parameters, such as a larger linear range and extra-low detection limit. The selectivity, stability, and reproducibility of these non-enzymatic sensors were successfully demonstrated. The practical utility of these sensors has demonstrated the quantification of H_2S, H_2O_2, and DA in real samples. These non-enzymatic sensors could be successfully detected the signaling molecules in different cancer cells such as breast cancer cells and glioma cells. This study paves the way for to design of efficient non-enzymatic electrochemical sensors for various biomolecules using a simple method. These nanomaterial-modified electrodes can be applied in in vivo models and implantation of these electrodes in the in vivo models is a great challenge. In the future, this is also a challenge to modify nanomaterials with microelectrodes to establish standard non-enzymatic electrodes for the detection of different signaling molecules.

Conclusion

1. Panda, Asit Kumar, et al. "Biocompatible Electrochemical Sensor Based on Platinum- Nickel Alloy Nanoparticles for In Situ Monitoring of Hydrogen Sulfide in Breast Cancer Cells." *Nanomaterials* 12.2 (2022): 258.
2. Li, Shanji, Asit Kumar Panda (Co-first author), Xinrui Liu, Yu-Chien Lin, Wen-Yen Huang, Chingpo Lin, Gang Zhao, and Ren-Jei Chung. "Preparation and biocompatibility studies of Collagen/Hyaluronic Acid/Oligomeric proanthocyanidins composites." Materials Chemistry and Physics 272 (2021): 124959.
3. Keerthi, Murugan, Asit Kumar Panda, Yao-Horng Wang, Xinke Liu, Jr-Hau He, and Ren- Jei Chung. "Titanium Nanoparticle Anchored Functionalized MWCNTs for Electrochemical Detection of Ractopamine in Porcine Samples with Ultrahigh Sensitivity." Food Chemistry (2022): 132083.
4. Tsai, Meng-Tsan, Ying-Sui Sun, Murugan Keerthi, Asit Kumar Panda, Udesh Dhawan, Yung-Hsiang Chang, Chih-Fang Lai, Michael Hsiao, Huey-Yuan Wang, and Ren-Jei Chung. "Oral Cancer Theranostic Application of FeAu Bimetallic Nanoparticles Conjugated with MMP-1 Antibody." *Nanomaterials* 12, no. 1 (2021): 61.
5. Liu X, Liu WC, Wang HY, Li VL, Chen YC, Wang AN, Wu CJ, Li Y, Zhao G, Lin C, Panda AK. Polyelectrolyte multilayer composite coating on 316 L stainless steel for controlled release of dual growth factors accelerating the restoration of bone defects. Materials Science and Engineering: C. 2021 Jul 1;126:112187.
6. Panda, A. K., Keerthi, ...& Chung, R. J. A Biocompatible Electrochemical Sensor Based on PtNi Alloy Nanoparticles Coupled N- GQDs for In Situ Monitoring of Dopamine in Glioma Cells. Materials Today Chemistry. (accepted, in press)
7. Panda, A. K., Keerthi, M., Sakthivel, R., Duann, Y. F., He, J. H., & Chung, R. J. A Non-Enzymatic, Biocompatible Electrochemical Sensor Based on N-doped Graphene Quantum Dot-Incorporated Sns2 Nanosheets for in Situ Monitoring of Hydrogen Peroxide in Breast Cancer Cells. Colloids and Surfaces B: Biointerfaces. (accepted, in press)

中技社 CTCI FOUNDATION